
A Triangular Network For Density Estimation

Xi-Lin Li
lixilinx@gmail.com

Abstract

We report a triangular neural network implementation of neural autoregressive flow (NAF). Unlike many universal autoregressive density models, our design is highly modular, parameter economy, computationally efficient, and applicable to density estimation of data with high dimensions. It achieves state-of-the-art bits-per-dimension indices on MNIST and CIFAR-10 (about 1.1 and 3.7, respectively) in the category of general-purpose density estimators.

1 Introduction

Probability density distribution (pdf) and conditional pdf estimations are topics of general interests, and also lie at the heart of many statistical learning and inference tasks. Traditional density estimation methods include histogram, kernel density estimation, orthogonal series density estimators, and finite mixture models (FMM) [1, 2, 3, 4]. These methods work well for data with low dimensions, but generally have difficulties when applied to data of high dimensions, i.e., the curse of dimensionality. Neural networks have achieved successes in many fields, and a few early examples of applying neural network to density estimations are independent component analysis (ICA) [5], Gaussianization [6] and [18]. Recently, there is a surge of neural network based density estimators. Many general-purpose neural network density estimators are based on autoregressive models, typically combining with normalizing flow, to name a few, neural networks for autoregressive density estimation (NADE) [18], masked autoencoder for distribution estimation (MADE) [7], masked autoregressive flow (MAF) for density estimation [8], neural autoregressive flows (NAF) [9], block neural autoregressive flow (B-NAF) [10], and unconstrained monotonic neural network (UMNN) [11]. Neural network density estimators can be designed for data with specific formats as well, e.g., non-linear independent components estimation (NICE) [12] and its successor, real NVP (Real NVP) [13], for images, where the correlations among neighboring pixels are hard-coded into the models. The neural ordinary differential equation (NODE) [14, 17] and its computationally cheaper version, free-form Jacobian of reversible dynamics (FFJORD) [16], provide yet another optimal transport based method for density estimation. These models and UMNN are different from traditional neural networks in the sense that they rely on numerical methods in both the train and inference phases. It is possible to combine several heterogeneous models to have hybrid, potentially more powerful, density estimators, e.g., the transformation autoregressive networks (TAN) [15]. Lastly, we recommend [21] for an overview of the more general normalizing flow based density estimation methods.

NAF looks like a promising direction for general-purpose density estimation. However, its previous implementations are never applied to high dimensional data [9, 10], possibly due to their high memory footprints. In this paper, we start from a simple two layer autoregressive network unit, and show that it is a universal approximator for invertible transformations with triangular Jacobians. Then, deep neural networks constructed by properly cascading such triangular network units and permutations are proposed as universal density estimators. Our method is closely related to NAF [9] and B-NAF [10]. But, we adhere to the simplest autoregressive network form to keep the model memory footprint to the minimum. This is essential for high dimensional density estimations.

2 Background

Here, we repeat a few well known facts to make our paper complete. This also serves to introduce our notations.

2.1 Probability density functions and change of variables

We consider two continuous random variable \mathbf{x} and \mathbf{y} connected by a smooth invertible mapping $\mathbf{f}(\cdot; \boldsymbol{\theta})$ with parameter vector $\boldsymbol{\theta}$ as

$$\mathbf{y} = \mathbf{f}(\mathbf{x}; \boldsymbol{\theta}) \quad (1)$$

The probability density functions of \mathbf{x} and \mathbf{y} , $p_X(\cdot)$ and $p_Y(\cdot)$ respectively, are related by

$$p_X(\mathbf{x}) = p_Y(\mathbf{y}) \left| \det \left(\frac{\partial \mathbf{y}}{\partial \mathbf{x}} \right) \right| \quad (2)$$

where $\nabla \mathbf{f} = \frac{\partial \mathbf{y}}{\partial \mathbf{x}}$ is called the Jacobian matrix, and $|\det(\cdot)|$ takes the absolute value of the determinant of a square matrix. Note that (2) is true only for invertible mappings.

Relationship (2), also referred to as normalizing flow in some work, is useful for density estimation and data generation. Assume that $p_X(\cdot)$ is unknown, but samples drawn from it are given. For $p_Y(\cdot)$ and $\mathbf{f}(\cdot; \boldsymbol{\theta})$ with proper forms, we can approximate $p_X(\cdot)$ by maximizing the empirical likelihood given by the right side of (2) with respect to $\boldsymbol{\theta}$ on samples drawn from $p_X(\cdot)$. On the other hand, the inverse mapping of $\mathbf{f}(\cdot; \boldsymbol{\theta})$, i.e., $\mathbf{x} = \mathbf{f}^{-1}(\mathbf{y}; \boldsymbol{\theta})$, provides a mean for sampling from $p_X(\cdot)$ indirectly. It is common to model $\mathbf{f}(\cdot; \boldsymbol{\theta})$ as neural networks due to their expressiveness.

2.2 Autoregressive model for density estimation

Assume that $\mathbf{x} = [x_1, x_2, \dots, x_N] \in \mathbb{R}^N$, where N is a positive integer. It is always feasible to factorize $p_X(\mathbf{x})$ recursively as

$$p_{X,1:n}(x_1, \dots, x_n) = p_{X,1:n-1}(x_1, \dots, x_{n-1}) p_{X,n|1:n-1}(x_n | x_1, \dots, x_{n-1}) \quad (3)$$

Correspondingly, it is possible to map each vector (x_1, \dots, x_n) to (y_1, \dots, y_n) successively for all $1 \leq n \leq N$ such that $p_Y(\mathbf{y})$ is factorized in the same fashion. Needless to say, all these N mappings should be invertible. Together, they define an autoregressive model. Noting that $\frac{\partial y_i}{\partial x_j} = 0$ for all $1 \leq i < j \leq N$, the Jacobian is a lower triangular matrix. This facilitates the calculation of its determinant, i.e.,

$$\det \left(\frac{\partial \mathbf{y}}{\partial \mathbf{x}} \right) = \prod_{n=1}^N \frac{\partial y_n}{\partial x_n} \quad (4)$$

Otherwise, calculating the determinant of an arbitrary dense matrix has complexity $\mathcal{O}(N^3)$. Hence, autoregressive model is one of the preferred choices for general-purpose density estimations with large N .

3 Monotonic triangular network

3.1 Monotonic triangular network unit

We consider a special two layer feedforward neural network defined as

$$\mathbf{y} = \mathbf{V}\phi(\mathbf{U}\mathbf{x} + \mathbf{a}) + \mathbf{b} \quad (5)$$

where both random variables \mathbf{x} and \mathbf{y} have the same dimension N , \mathbf{U} and \mathbf{V} are two lower triangular block matrices with block sizes $(B, 1)$ and $(1, B)$, respectively, B is a positive integer, and set $\{\mathbf{U}, \mathbf{V}, \mathbf{a}, \mathbf{b}\}$ collects all the trainable parameters. Clearly, Jacobian $\frac{\partial \mathbf{y}}{\partial \mathbf{x}}$ is a lower triangular matrix as well. Let the n th diagonal blocks of \mathbf{U} and \mathbf{V} be $[u_{n,1}, u_{n,2}, \dots, u_{n,B}]$ and $[v_{n,1}, v_{n,2}, \dots, v_{n,B}]$, respectively. Then, we have

$$\frac{\partial y_n}{\partial x_n} = \sum_{i=1}^B u_{n,i} v_{n,i} \dot{\phi}_{(n-1)B+i}, \quad 1 \leq n \leq N \quad (6)$$

where $\dot{\phi}_{(n-1)B+i}$ is the derivative of the $[(n-1)B+i]$ th nonlinearity (activation function) in ϕ . To simplify the notations, we do not explicitly show $\dot{\phi}_{(n-1)B+i}$'s dependence on \mathbf{U} , \mathbf{x} and \mathbf{a} . An interesting observation is that when $\phi_{(n-1)B+i}$ is monotonically increasing, and $u_{n,i}$ and $v_{n,i}$ have the same or opposite sign for all $1 \leq i \leq B$, $\frac{\partial y_n}{\partial x_n}$ will always be either positive or negative. Then, y_n must be monotonic with respect to x_n . This observation is true for all $1 \leq n \leq N$. Hence, (5) defines a monotonic network when ϕ is element-wisely monotonically increasing, and each group of $u_{n,i}$ and $v_{n,i}$ for $1 \leq i \leq B$ have the same or opposite sign. The following proposition states that such networks can approximate any invertible mappings with triangular Jacobians. The proof should be straightforward following the universal approximation theorem and the fact that networks with positive weights can approximate any continuous monotonic mappings [20]. Here, we sketch an informal one to make our report complete.

Proposition 1: The neural network defined in (5) can approximate any continuous invertible mapping on a compact subset of \mathbb{R}^N with lower triangular Jacobians arbitrarily well when C1) B is sufficiently large; C2) each group of $u_{n,i}$ and $v_{n,i}$, $1 \leq i \leq B$, have the same or opposite sign for all $1 \leq n \leq N$; C3) all the nonlinearities in ϕ are monotonically increasing, and lower and upper bounded.

Proof: The universal approximation theorem ensures that without imposing the sign constraints on the block diagonals of \mathbf{U} and \mathbf{V} , the network defined in (5) can approximate any continuous mapping with triangular Jacobian. Hence, we only need to show that y_n can approximate any mapping monotonic with respect to x_n , or equivalently, $\frac{\partial y_n}{\partial x_n}$ can approximate any scalar function of (x_1, \dots, x_n) whose outputs always have the same sign. Let us rewrite y_n and $\frac{\partial y_n}{\partial x_n}$ explicitly as below

$$y_n = \sum_{i=1}^B v_{n,i} \phi_{(n-1)B+i}(u_{n,i}(x_n - c_i(x_1, \dots, x_{n-1}))) + (\text{a bias constant}) \quad (7)$$

$$\frac{\partial y_n}{\partial x_n} = \sum_{i=1}^B u_{n,i} v_{n,i} \dot{\phi}_{(n-1)B+i}(u_{n,i}(x_n - c_i(x_1, \dots, x_{n-1}))) \quad (8)$$

where c_i , $1 \leq i \leq B$, are B scalar functions of (x_1, \dots, x_{n-1}) introduced after reparameterization. Without loss of generality, we assume that for all $1 \leq i \leq B$, $\phi_{(n-1)B+i}$ is bounded as $\phi_{(n-1)B+i}(-\infty) = 0$ and $\phi_{(n-1)B+i}(\infty) = 1$, and $u_{n,i}$ and $v_{n,i}$ are positive, i.e., y_n is monotonically increasing with respect to x_n . Then, for sufficiently large $u_{n,i}$, we have

$$\lim_{u_{n,i} \rightarrow \infty} u_{n,i} \dot{\phi}_{(n-1)B+i}[u_{n,i}(x_n - c_i(x_1, \dots, x_{n-1}))] = \delta(x_n - c_i(x_1, \dots, x_{n-1})) \quad (9)$$

where $\delta(\cdot)$ is the Dirac delta function. Now, let us consider an arbitrary continuous scalar mapping $(x_1, x_2, \dots, x_n) \mapsto g(x_1, x_2, \dots, x_n) > 0$. It is clear that any value $g(z_1, z_2, \dots, z_n)$ can be approximated by letting $u_{n,i} v_{n,i} = g(z_1, z_2, \dots, z_n)$ and $c_i(x_1, \dots, x_{n-1})$ be a function that equals z_n only when $(x_1, \dots, x_{n-1}) = (z_1, \dots, z_{n-1})$, which is feasible due to the universal approximation theorem. Thus, (8) is dense on a compact set when B is sufficiently large. This finishes the proof. \square

Let us check each condition used in the above proof closely. C1) is quite standard. C2) arises naturally as outputs of the target mapping have the same sign. C3) is used in (9). Intuitively, we see that the right side of (6) is a weighted sum of the shifted and rescaled versions of the derivative of nonlinearity $\phi_{(n-1)B+i}$. Under mild conditions, these shifted and rescaled derivatives form an over complete base for function approximation, as illustrated in Fig. 1 for the case with dimension 1. However, unbounded nonlinearities are widely used in today's neural networks, e.g., the rectified linear unit (ReLU). Unfortunately, it is not difficult to show that such nonlinearities do not work here. The derivative of ReLU is monotonic. Hence, derivative of its weighted sum is monotonic as well as long as the weights have the same sign. But, not all monotonic functions have monotonic derivatives. Thus, any nonlinearities with monotonic derivatives cannot be used here.

3.2 Unconstrained monotonic network for density estimation

For density estimation, it is sufficient to constrain $u_{n,i}$ and $v_{n,i}$ to be positive for all $1 \leq n \leq N$ and $1 \leq i \leq B$. It could be inconvenient to keep all these positiveness constraints on the block diagonals of \mathbf{U} and \mathbf{V} . But, it is trivial to reparameterize them to drop off these constraints. In our implementations, we choose reparameterization

$$u_{n,i} = -\log \sigma(-\mu_{n,i}), \quad v_{n,i} = -\log \sigma(-\nu_{n,i}), \quad 1 \leq n \leq N, \quad 1 \leq i \leq B \quad (10)$$

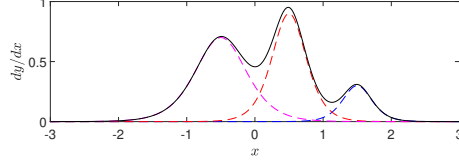


Figure 1: A positive scalar function (solid line) is approximated as the sum of three shifted and rescaled versions of the derivative of tanh (dotted lines).

where $\sigma(\cdot)$ is the sigmoid function, and $\mu_{n,i}$ and $\nu_{n,i}$ are free to take any real values. Hyperparameter B can be viewed as the order of our monotonic triangular network unit. Note that memory footprint of a unit is proportional to B . Regarding ϕ , commonly used squash functions, e.g., the sigmoid and tanh, will work since they are monotonic and bounded. Certain unbounded nonlinearities, e.g., ReLU, should be avoided per our above discussions.

It is a common practice to choose $p_Y(\mathbf{y})$ as a standard normal density. Then, given samples \mathbf{x} from an unknown distribution $p_X(\cdot)$, we can estimate it in the form of (2) by minimizing expectation of the following negative-logarithm-likelihood (NLL)

$$-\sum_{n=1}^N \log \frac{\partial y_n}{\partial x_n} + 0.5 \mathbf{y}^T \mathbf{y} + 0.5N \log(2\pi) \quad (11)$$

with respect to parameters $\{\mathbf{U}, \mathbf{V}, \mathbf{a}, \mathbf{b}\}$. On the other hand, a monotonic network unit can be reversed in a way similar to backward substitution for solving linear triangular equations, i.e., solving for x_n when (x_1, \dots, x_{n-1}) are ready. As y_n is monotonic with respect to x_n , simple root finding methods like bisection could be sufficient for solving for x_n given y_n and (x_1, \dots, x_{n-1}) .

Lastly, deep neural networks obtained by stacking several monotonic triangular network units are still monotonic, have triangular Jacobians, and can be inverted with a backward substitution like routine as well. Such networks might look superficially similar to the B-NAF in [10]. But, there are a few subtle differences. We do not apply any nonlinear mapping on the outputs of each monotonic triangular network unit. Intuitively, squashing will deviate outputs of a unit away from normal distribution, which conflicts with our aim. Memory footprint of each unit is proportional to its order B . This avoids the memory explosion issue caused by those wide intermediate layers in B-NAF. A few implementation tips proposed in the next section further enhance the usefulness of this design for high dimensional density estimation.

4 Practical triangular networks for density estimation and data generation

Here, we prescribe a few modifications to the monotonic triangular networks in Section 3 to enhance its usefulness in practice.

4.1 Non-autoregressive model by inserting permutations

Although a large enough monotonic triangular network suffices to universal density estimation, it is unlikely the case that autoregressive model is parameter economy for all density estimation tasks. In general, we can obtain deep reversible non-autoregressive models by cascading monotonic triangular network units and permutations as below

$$\mathbf{x}_0 \rightarrow \boxed{\text{MonoTriNetU}} \rightarrow \boxed{\text{P}} \xrightarrow{\mathbf{x}_1} \boxed{\text{MonoTriNetU}} \rightarrow \boxed{\text{P}} \xrightarrow{\mathbf{x}_2} \dots \xrightarrow{\mathbf{x}_{L-1}} \boxed{\text{MonoTriNetU}} \rightarrow \boxed{\text{P}} \xrightarrow{\mathbf{x}_L}$$

where each $\boxed{\text{MonoTriNetU}}$ and $\boxed{\text{P}}$ denote an independent monotonic triangular network unit and permutation unit, respectively. Due to these inserted permutations, the Jacobian $\frac{\partial \mathbf{x}_L}{\partial \mathbf{x}_0}$ is no longer ensured to be triangular. However, it is still convenient to calculate its determinant as

$$\det \left(\frac{\partial \mathbf{x}_L}{\partial \mathbf{x}_0} \right) = \prod_{\ell=1}^L \det \left(\frac{\partial \mathbf{x}_\ell}{\partial \mathbf{x}_{\ell-1}} \right) = \prod_{\ell=1}^L \prod_{n=1}^N \frac{\partial x_{\ell,n}}{\partial x_{\ell-1,n}} \quad (12)$$

where we have used the fact that the determinant of a permutation matrix is 1. Different from a monotonic triangular network, a one-pass backward substitution like inversion no longer works here. Instead, we need to inverse each permutation and monotonic triangular network unit step by step, down from the top layer to the bottom layer.

Let us check the network

$$\mathbf{x} \rightarrow \boxed{\text{MonoTriNetU}} \rightarrow \boxed{\text{Flip}} \rightarrow \boxed{\text{MonoTriNetU}} \rightarrow \boxed{\text{Flip}} \xrightarrow{\mathbf{y}} \quad (13)$$

to see why permutation could help, where $\boxed{\text{Flip}}$ is the permutation that reverses the order of a vector. Mathematically, we have $\mathbf{y} = \mathbf{F}\mathbf{f}_2(\mathbf{F}\mathbf{f}_1(\mathbf{x}))$, where $\mathbf{F} = \text{antidiag}(1, 1, \dots, 1)$ is the unit anti-diagonal matrix, and $\mathbf{f}_1(\cdot)$ and $\mathbf{f}_2(\cdot)$ are two independent monotonic triangular network units. Its Jacobian is

$$\frac{\partial \mathbf{y}}{\partial \mathbf{x}} = (\mathbf{F}\nabla \mathbf{f}_2 \mathbf{F}) \nabla \mathbf{f}_1 \quad (14)$$

where $\nabla \mathbf{f}_1$ is a lower triangular matrix, and $\mathbf{F}\nabla \mathbf{f}_2 \mathbf{F}$ is an upper triangular one. We know that a constant square matrix can be factorized as the product of an upper triangular matrix and a lower one¹. Similarly, we expect that the upper-lower decomposition form in (14) can approximate the Jacobians from a larger family of invertible mappings.

4.2 Bijective network with a ‘log’ nonlinearity for data generation

It is worthy to point out that with a finite B and bounded nonlinearities, (5) only defines an injective mapping on \mathbb{R}^N . Specifically, with nonlinearity ‘tanh’, we have $|y_n| < \sum_{i=1}^B |v_{n,i}|$. Thus, when the target distribution is a standard normal one, it is not possible to invert all samples drawn from $p_Y(\cdot)$. Although the probability measure of such non-invertible samples could be negligibly small for good enough density models, this brings inconveniences for applications like data generation. Here, we propose to replace a bounded nonlinearity with a ‘log’ nonlinearity, $\text{sign}(x) \log(1 + |x|)$, when bijection is a must. This ‘log’ nonlinearity is neither lower nor upper bounded. It is easy to show that the networks in Section 4.1 become bijective on \mathbb{R}^N after adopting it. Our experiences suggests that the ‘log’ nonlinearity behaves similar to a squash one since its output amplitudes grow slowly enough with respect to its inputs. It even could outperform the tanh nonlinearity in negative-logarithm-likelihood performance index when B is too small and $p_Y(\cdot)$ is the standard normal density. This is not astonishing since the sum of a few hard bounded terms cannot fit well with the tails of a normal distribution.

4.3 Compact model storage

Two strategies are used to save our neural networks compactly. First, instead of saving the two triangular matrices in (5) separately, we save most of their elements compactly in a dense matrix. Let $\text{off}(\mathbf{V}) = \mathbf{V} - \text{bdiag}(\mathbf{V})$, where $\text{bdiag}(\mathbf{V})$ is the block diagonals of \mathbf{V} . Then, we can put $\text{off}(\mathbf{V}^T)$ in the upper triangular part of \mathbf{U} to save memory. The block diagonals of \mathbf{V} is saved as a separate vector. Second, we generate the masks for exacting \mathbf{U} and $\text{off}(\mathbf{V}^T)$ from the dense matrix they are nested in on the fly. Note that B , and thus the masks, can be inferred from the sizes of \mathbf{U} and \mathbf{V} . Thus, there is no need to save them in advance. These two strategies reduce the model memory footprint to about one fourth of value required by naively saving \mathbf{U} , \mathbf{V} and their masks in separated matrices. Clearly, it is the design regularity of our monotonic triangular network unit to make such significant storage reduction possible.

4.4 Linear autoregressive input normalization

Lastly, it is known that input normalization generally helps to facilitate training. We propose to use a linear autoregressive model to preprocess the input as $\mathbf{x} \leftarrow \mathbf{\Gamma}(\mathbf{x} - \mathbf{m})$, where \mathbf{m} and \mathbf{C} are the (empirical) mean and covariance matrix of \mathbf{x} , respectively, and $\mathbf{\Gamma}$ is a lower triangular matrix given by Cholesky decomposition $\mathbf{C}^{-1} = \mathbf{\Gamma}^T \mathbf{\Gamma}$. Unlike the more popular principle component analysis (PCA) based whitening preprocessing, this one works seamlessly with our neural network since itself is a simple autoregressive unit. The preprocessing parameters, \mathbf{m} and $\mathbf{\Gamma}$, have no need to be exact, nor need to be adapted during the training, since they could be absorbed into the input layer of the

¹The product sometimes includes a permutation matrix as well.

Table 1: Test bits-per-dimension comparison on image density estimation benchmarks.

| | MNIST | CIFAR-10 |
|-----------------------------------|-----------------|-----------------|
| Best of MADE/MoG [8] | 1.41 ± 0.01 | 5.67 ± 0.01 |
| Best of Real NVP [8] | 1.93 ± 0.01 | 4.53 ± 0.01 |
| Best of MAF/MoG [8] | 1.52 ± 0.01 | 4.31 ± 0.01 |
| TAN [15] | 1.19 | 3.98 |
| UMNN [11] | 1.13 ± 0.02 | — |
| TriNet , L1 regularization | 1.13 | 3.70 |
| TriNet , augmentation | 1.09 | 3.69 |

first monotonic triangular network unit as $\mathbf{U} \leftarrow \mathbf{U}\mathbf{T}$ and $\mathbf{a} \leftarrow \mathbf{a} - \mathbf{U}\mathbf{T}\mathbf{m}$. Indeed, They will not show up in the trained and finalized model coefficients after being absorbed.

5 Experimental Results

Pytorch implementation of our method and more experimental results can be found at <https://github.com/lixilinx/TriNet4PdfEst>. Here, we report the density estimation results for MNIST and CIFAR-10 data sets. The label information is discarded. The pixel values in space $[0, 255]^N$ are first dequantized by adding uniform noise $\mathcal{U}(0, 1)$, then rescaled to range $[0, 1]$, and finally transferred to the logit space with mapping $x \mapsto \text{logit}(\lambda + (1 - 2\lambda)x)$, where $\lambda = 10^{-6}$ and 0.05 for MNIST and CIFAR-10, respectively. We estimate the density in the logit space, but report the bits-per-dimension performance index for comparison as it is more popular than the negative-logarithm-likelihood one.

We have trained invertible triangular networks consists of four cascaded monotonic units with different settings. Block sizes are 100 and 8 for MNIST and CIFAR-10, respectively. Batch size is 64 in both tasks. All models are trained with Adam starting from initial step size 10^{-4} . We reduce the step size by one order of magnitude when no performance improvement is observed on the validation set. The train, validation and test sets are defined following the ways in [8]. We find that our model could seriously overfit the CIFAR-10 dataset even with early stopping and such a small B (about 0.5 bits-per-dimension gap between train and validation set). We have tried two ways to alleviate overfitting, L1 regularization and train data augmentation by randomly and circularly shifting the images up to $[0.1 \times (\text{image size})]$ pixels both horizontally and vertically. Detailed negative-logarithm-likelihood and bits-per-dimension indices on train, validation and test sets under different settings are summarized in Appendix A. Table 1 summarizes the test results for comparison. Standard deviations of our method are not listed as all are below 0.01. Note that only those general-purpose density estimators are compared here. Density estimators specifically designed for images could perform better [21]. From Tabel 1, we see that our models outperform their competitors by great margins, especially on the CIFAR-10 task.

Randomly generated handwritten digits and image patches drawn from the MNIST and CIFAR-10 density models trained with L1 regularization are posted in Appendix B. Models trained with augmented data are not used here since their performances on train set are worse than the ones with L1 regularization (see Appendix A). Most digit samples are recognizable, although less generated image patches make sense to a human subject.

References

- [1] B. W. Silverman, *Density Estimation for Statistics and Data Analysis*. London: Chapman and Hall, 1986.
- [2] J. E. Kolassa, *Series Approximation Methods in Statistics*, 3rd Edition. New York: Springer, 2006.
- [3] A. J. Izenman, Recent developments in nonparametric density estimation. J. Amer. Statist. Assoc., vol. 86, pp. 205–225, 1991.
- [4] G. J. McLachlan, *Finite Mixture Models*, Wiley, 2000.

- [5] H. Aapo and E. Oja. Independent component analysis: algorithms and applications. *Neural Networks*, no. 4–5, vol. 13, pp. 411–430, 2000.
- [6] S. S. Chen and R. A. Gopinath. Gaussianization. In *Proceedings of NIPS*, 2000.
- [7] M. Germain, K. Gregor, I. Murray, and H. Larochelle. Made: masked autoencoder for distribution estimation. In *International Conference on Machine Learning*, pages 881–889, 2015.
- [8] G. Papamakarios, T. Pavlakou, and I. Murray. Masked autoregressive flow for density estimation. In *Advances in Neural Information Processing Systems*, pages 2338–2347, 2017.
- [9] C. W. Huang, D. Krueger, A. Lacoste, and A. Courville. Neural autoregressive flows. In *International Conference on Machine Learning*, pages 2083–2092, 2018.
- [10] N. De Cao, I. Titov, and W. Aziz. Block neural autoregressive flow. *arXiv preprint, arXiv:1904.04676*, 2019.
- [11] A. Wehenkel, and G. Louppe, Unconstrained monotonic neural networks. In *Conference on Neural Information Processing Systems*, Vancouver, Canada, 2019.
- [12] L. Dinh, D. Krueger, and Y. Bengio. NICE: non-linear independent components estimation. In *International Conference on Learning Representations (ICLR)*, 2015.
- [13] L. Dinh, J. Sohl-Dickstein, and S. Bengio. Density estimation using Real NVP. In *International Conference on Learning Representations*, 2017.
- [14] T. Q. Chen, Y. Rubanova, J. Bettencourt, and D. K. Duvenaud. Neural ordinary differential equations. In *Advances in Neural Information Processing Systems*, pages 6571–6583, 2018.
- [15] J. Oliva, A. Dubey, M. Zaheer, B. Poczos, R. Salakhutdinov, E. Xing, and J. Schneider. Transformation autoregressive networks. In *International Conference on Machine Learning*, pp. 3895–3904, 2018.
- [16] W. Grathwohl, R. T. Chen, J. Bettencourt, I. Sutskever, and D. Duvenaud. FFJORD: free form continuous dynamics for scalable reversible generative models. In *International Conference on Machine Learning*, 2018.
- [17] L. Zhang, W. E. and L. Wang. Monge-Ampère flow for generative modeling. *arXiv preprint, arXiv:1809.10188*, 2018.
- [18] H. Larochelle, and I. Murray. The neural autoregressive distribution estimator. In *Proceedings of the Fourteenth International Conference on Artificial Intelligence and Statistics*, pp. 29–37, 2011.
- [19] M. M. Ismail and A. Atiya. Neural networks for density estimation. In *Advances in Neural Information Processing Systems*, pages 522–528, 1999.
- [20] H. Daniels, and M. Velikova, Monotone and partially monotone neural networks. *IEEE Transactions on Neural Networks*, no. 6, vol. 21, pp. 906–917, 2010.
- [21] I. Kobyzev, S. J. D. Prince, and M. A. Brubaker. Normalizing flows: an introduction and review of current methods. *arXiv preprint, arXiv:1908.09257v3*, 2020.

Appendix A: further density estimation results

A1: Optional setups

Nonlinearity (activation function): either tanh or log, i.e., $\text{sign}(x) \log(1 + |x|)$.

Optional permutation: flipping the outputs of each monotonic triangular network unit.

L1 regularization term: $\eta \times (\text{sum of the absolute values of model coefficients})$, where $\eta > 0$. L1 regularization encourages sparse connections, which imply sparse dependence structures in the data.

Optional data augmentation: randomly and circularly shift the train images up to $\lfloor 0.1(\text{image size}) \rfloor$ pixels both horizontally and vertically.

Note that the negative-logarithm-likelihood indices from different methods might not be directly comparable due to different processing. However, the bits-per-dimension indices are always comparable.

A2: Results without regularization and augmentation

We reduce the training step size when no validation performance gain is observed after 10 and 5 successive epochs for MNIST and CIFAR-10, respectively. Flipping generally helps for CIFAR-10, but not for MNIST. It makes sense as most people write digits from the top left corner down to the bottom right corner, comparable to an autoregressive generative model. The ‘log’ nonlinearity significantly outperforms the tanh one on the

CIFAR-10 task, perhaps due to a small B . Huge performance gaps between train and validation sets on the CIFAR-10 task suggest serious overfitting.

Table 2: Negative-logarithm-likelihood (bits-per-dimension), w/o regularization, w/o augmentation

| | Train | MNIST Validation | Test | Train | CIFAR-10 Validation | Test |
|----------------|-----------|---------------------|-----------|-------------|------------------------|-------------|
| w/o flip, tanh | 654(1.06) | 703(1.15) | 698(1.14) | -4515(3.62) | -3558(4.07) | -3523(4.09) |
| w/o flip, log | 680(1.11) | 709(1.16) | 705(1.16) | -4584(3.59) | -3719(3.99) | -3744(3.98) |
| w flip, tanh | 706(1.16) | 721(1.18) | 716(1.18) | -4490(3.63) | -3401(4.14) | -3453(4.12) |
| w flip, log | 692(1.13) | 725(1.19) | 722(1.19) | -4828(3.47) | -3804(3.96) | -3810(3.95) |

A3: Results without regularization and with augmentation

We reduce the training step size when no validation performance gain is observed after 10 and 5 successive epochs for MNIST and CIFAR-10, respectively. Again, flipping helps for CIFAR-10, but not for MNIST. This data augmentation method seems quite coarse. Over fitting is avoid, but performances on the train sets drop a lot, compared with those from Table 2.

Table 3: Negative-logarithm-likelihood (bits-per-dimension), w/o regularization, w augmentation

| | Train | MNIST Validation | Test | Train | CIFAR-10 Validation | Test |
|----------------|-----------|---------------------|------------------|-------------|------------------------|--------------------|
| w/o flip, tanh | 676(1.10) | 677(1.10) | 674(1.10) | -4150(3.79) | -4135(3.80) | -4126(3.80) |
| w/o flip, log | 674(1.10) | 675(1.10) | 672(1.09) | -4166(3.78) | -4184(3.77) | -4152(3.79) |
| w flip, tanh | 706(1.16) | 707(1.16) | 703(1.15) | -4282(3.73) | -4286(3.73) | -4261(3.74) |
| w flip, log | 721(1.18) | 722(1.19) | 717(1.18) | -4387(3.68) | -4391(3.68) | -4365(3.69) |

A4: Results with regularization and without augmentation

We reduce the training step size when no validation performance gain is observed after 10 successive epochs. We try η with possible values from set $\{\dots, 10^{-3}, 10^{-4}, 10^{-5}, \dots\}$, and choose the one performing the best on validation set. L1 regularization factors are 10^{-4} and 10^{-3} for MNIST and CIFAR-10, respectively. It looks like that regularization improves the MNIST training performance when compared with Table 2. This is caused by different early stopping conditions. Actually, the train performance indices on both tasks can go further down without early stopping.

Table 4: Negative-logarithm-likelihood (bits-per-dimension), w regularization, w/o augmentation

| | Train | MNIST Validation | Test | Train | CIFAR-10 Validation | Test |
|----------------|-----------|---------------------|------------------|-------------|------------------------|--------------------|
| w/o flip, tanh | 647(1.05) | 694(1.13) | 690(1.13) | | | |
| w/o flip, log | | | | | | |
| w flip, tanh | | | | | | |
| w flip, log | | | | -4649(3.56) | -4324(3.71) | -4351(3.70) |

Appendix B: randomly generated image samples

B1: MNIST samples

B2: CIFAR-10 samples

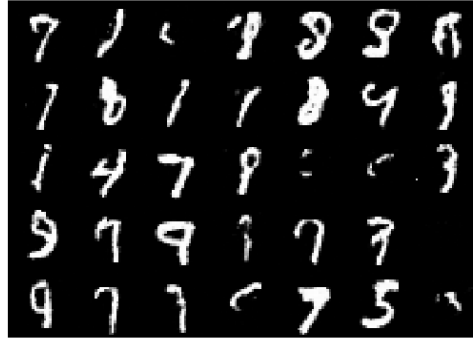


Figure 2: 35 randomly generated handwritten digit images drawn from the MNIST density model trained with L1 regularization.

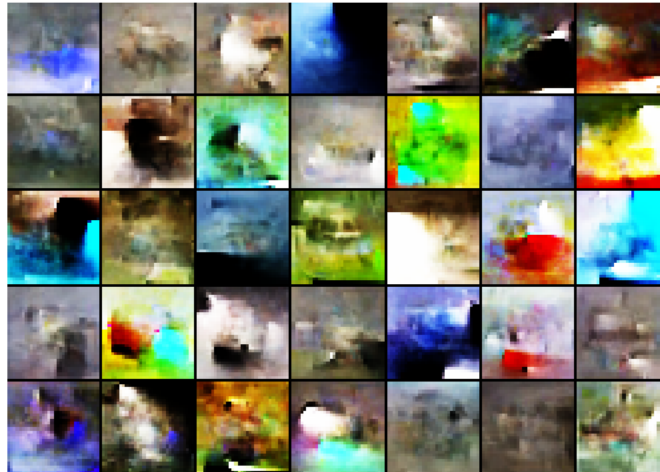


Figure 3: 35 randomly generated image patches drawn from the CIFAR-10 density model trained with L1 regularization. A few look recognizable, e.g., the last one looks like a frog.